A RADAR-ECHO MODEL FOR MARS; T.W. Thompson, Calif. Inst. Tech., Jet Propulsion Laboratory, Pasadena, CA, 96011 and H.J. Moore, U.S. Geological Survey, Menlo Park, CA, 94025.

We have developed a radar-echo model for Mars based on 12.6-cm continuous-wave radio transmissions backscattered from the planet [1,2]. Our model (1) broadly matches the variations in depolarized and polarized total-radar cross sections with longitude observed by Goldstone in 1986 along 7° S. and (2) yields echo spectra that are generally similar to the observed spectra, with some departures.

In our model, Mars' surface is divided into radar map units that are based on generalized geologic map units [2]; the radar map units are further subdivided using thermal inertias [3]. Thermal inertias are used because the geologic map units are not sufficient to account for the quasi-specular echoes and normal reflectivities and thermal inertias are positively correlated along 7° S. and elsewhere [4,5]. For cratered uplands and plains units, model depolarized- echo strengths vary as A*cos[theta] (where [theta] is the incidence angle and A is a parameter assigned to the radar map unit on a degree by degree basis), and polarized diffuse-echo strengths vary as 3*A*cos[theta]. For most volcanic units, depolarized and polarized diffuse-echo strengths vary as $A*\cos^2[\text{theta}]$. Quasi-specular echoes were computed using Hagfors' scattering law [6] (integrated from -30° to +30° theta). Assignments of depolarized echo strengths, normal reflectivities, and root-mean-square (rms) slopes for the radar map units were guided by previous experience [2], thermal inertias [3], and the results from analyses of the quasi-specular echo spectra and then they were adjusted by trial and error methods to best fit the data. Coarse-scale topography is not included in the model.

Radar map units in our model include: (1) an extensive cratered uplands (background) unit with weak depolarized echo cross sections (0.01), average thermal inertias, moderate normal reflectivities (0.095), and moderate rms slopes (4.0°); (2) the volcanic units of the Tharsis, Elysium, and Amazonis regions with strong depolarized echo cross sections (0.04-0.133), low thermal inertias, low normal reflectivities (0.025-0.050), and large rms slopes (6-20°); and (3) the northern plains units with moderate to strong depolarized echo cross sections (0.017-0.045), moderate to very high thermal inertias, moderate to large normal reflectivities (0.075-0.15), and moderate rms slopes (3-5°). Arabia, an extensive unit of upland that is mantled by dust, has a low depolarized-echo cross section (0.007), low thermal inertia, small normal reflectivity (0.05), and small rms slope (3.0°). There are additional radar map units (there are about 140 radar map units). At this time, our model does not include an equatorial region extending from the vicinity of western Pavonis Mons to S.E. Elysium Planitia that has non-existent to very weak depolarized echoes or the very strong ones from the poles

observed at 3.6-cm wavelength [7].

Like the observations, model total-polarized echo cross sections vary with longitude as a two-cycle curve with maxima near 30° and 240° W. and minima near 130° and 330° W.; model total-depolarized-echo cross sections vary with longitude as a one-cycle curve with a maximum near 135° and a minimum near 330° W.; and, the ratio of total-depolarized and total-polarized cross sections (mu) vary with longitude as a one-cycle curve.

Model depolarized- and polarized-echo spectra, as well as ratios of the two, resemble those that are observed. For smooth regions with moderate thermal inertias and normal reflectivities, the central parts of polarized-echo spectra are dominated by the quasi-specular parts that form tall, narrow peaks that rest upon low, broad domes of the diffuse echoes. In rough regions with low thermal inertias and small normal reflectivities, the quasi-specular echoes form low broad peaks that rest upon and merge imperceptibly with the broad domes of the diffuse part of the echoes. Like the observed spectra, the forms of the polarized diffuse echoes tend to mimic the depolarized echoes except near the centers of the spectra where the quasi-specular parts of the polarized echoes totally dominate the spectra. For the model and observations, ratios of the spectra of depolarized and polarized echoes are similar.

Several aspects of our model are instructive and relevant to the interpretation of radar echoes from Mars. These aspects are related to the sizes of the heterogeneous radar map units areas sampled by the radar, and the way in which the radar samples the surface; for example: (1) quasi-specular echoes from horizontal surfaces may be asymmetrical with peaks displaced from zero-doppler frequency when the radar samples adjacent units with different roughnesses; (2) quasi-specular echoes from very smooth areas with embedded very rough areas may be so dominated by the smooth areas that the rough areas are not revealed in the spectra; and (3) the diffuse parts of the polarized echoes may contribute substantially to the polarized echoes. Careful examination of observed echoes show that the surface of Mars is, like our model, heterogeneous.

REFERENCES

[1] Thompson, T.W., 1988, LPI Tech. Report 88-05, p. 107-108. [2] Thompson, T.W. and Moore, H.J., 1989, Proc. 19th Lunar and Planet. Sci. Conf., p. 409-422. [3] Palluconi, F.D. and Kieffer, H.H., 1981, Icarus, v. 45, p. 415-426. [4] Jakosky, B.M. and Christensen, P.R., 1986, Icarus, v. 66, p. 125-133. [5] Moore, H.J. and Jakosky, B.M., 1989, Icarus, v. 81, p. 164-184. [6] Hagfors, T., 1964, J. Geophys. Res., v. 69, p. 3779-3784. [7] Butler, B., Muhleman, D., Grossman, A., and Slade, M., 1989, Eos (Trans. Am. Geophys. Union), v. 70, #43, p. 1171.

IMPLICATIONS OF CRUSTAL FORMATION ON MARS FROM PARAMETERIZED CONVECTION CALCULATIONS

D.L. Turcotte and J. Huang, Department of Geological Sciences, Cornell University, Ithaca, NY 14853

In order to better understand the evolution of Mars we have carried out a series of parameterized convection calculations (1). An important aspect of our analyses is the removal of the heat producing elements from the Martian mantle to the crust. The rate of crustal formation is calibrated using the present rate of crustal generation on the earth and the moon. The evolution of the mean mantle temperature, crustal thickness, lithosphere thickness, rate of volcanism, mantle heat flow, change of radius, and Urey number are obtained. Several studies (2-4) utilizing gravity anomalies and Airy compensation have suggested that the thickness of the Martian crust is 115-130 km. This is consistent with our results if the crustal fractionation parameter is in the range 0.0025-0.005. These are somewhat lower than the values inferred for the earth and moon which are near 0.001.

Accepting that the crustal fractionation factor for Mars is 0.003, we can determine rates of volcanism. The average amount of crust added in the last billion years (0-1 Gyr BP) is predicted to be 600 m, the average amount of crust added between 1-2 Gyr BP was 1.8 km, and the average amount of crust added between 2-3 Gyr BP was 2.9 km.

A detailed summary of the stratigraphy of Mars has been given by Tanaka (5). Relative ages are quite tightly constrained by crater counts, but absolute ages are uncertain due to uncertainties in the volcanic flux. The most recent volcanism is associated with the Upper Amazonian period. Volcanics of this period are associated with the Arcadra, Olympus Mons, Medusae Fossae, and Tharsis Montes Formations but the principal volcanics are flood basalts in the southern Elysium Planitia. These have an area of 100,000 km^2 but Tanaka (5) suggests that the thickness is only a few tens of meters. Taking a thickness of 50 m this is only 0.03 m when averaged over the surface of Mars.

Greeley (6) has estimated that 26×10^6 km^3 of volcanics erupted during the Middle and Upper Amazonian. This corresponds to a mean thickness of 200 m when averaged over the entire surface

of Mars. Based on the meteorite flux intensity given by Hartmann et al (1981) the Upper Amazonian extends from 0 to 0.7 Gyr BP and the Middle Amazonian from 0.7 to 2.3 Gyr BP. Thus the Young volcanoes on Mars are consistent with our results. It should be emphasized, however, that there are considerable uncertainties in the absolute ages.

Other predictions of our calculations using $\chi = 0.003$ are that the lithosphere thickness $D_L = 400$ km, the Urey Number = 0.7, and a net contraction corresponding to $\delta r/r = -0.001$. We predict that a global expansion of $\delta r = 10$ km occurred in the first 200 Myr of the evolution of Mars. This expansion was caused by the density change associated with the generation of the early crust. For the remainder of the evolution of Mars a nearly steady contraction occurred associated with the cooling of the interior. The total contraction was $\delta r = -13$km.

The surface tectonic features of Mars include both extensional features and compressional features. Much of the evidence for lithospheric extension on Mars is provided by graben systems in and near the Tharsis region. These features are likely to be the result of the stresses generated by the Tharsis load. Wrinkle ridges occur commonly throughout ancient terrains. These can be attributed to thermal contraction.

References:

(1) Turcotte, D.L., et al., Proc. Lunar Planet. Sci. Conf. 10th, 2375-2392, 1979. (2) Sjogren, W.J. and R.N. Wimberly, Icarus 45, 331-338, 1981. (3) Sjogren, W.J. and S.J. Ritke, Geophys. Res. Let. 9, 739-742, 1982. (4) Janle, P., Moon Planets 28, 55-67, 1983. (5) Tanaka, K.L., J. Geophys. Res., 91, E139-E158, 1986. (6) Greeley, R., Science 236, 1653-1654, 1987. (7) Hartmann, W.K., et al., Basaltic Volcanism, 1049-1127, 1981.

THE NATURE AND ORIGIN OF PERIODICALLY SPACED WRINKLE RIDGES ON MARS. Thomas R. Watters, Center for Earth and Planetary Studies, National Air and Space Museum, Smithsonian Institution, Washington, D.C. 20560.

Over 3% of the surface of Mars is covered by smooth plains material characterized by landforms analogous to mare wrinkle ridges. Although the exact nature of these ridged plains materials has not been directly determined, indirect evidence suggests they are the result of flood volcanism (1,2,3). The origin of wrinkle ridges is also not agreed upon, and recent debates have focused on the role of buckling and reverse or thrust faulting (3,4,5). However, the general consensus is that wrinkle ridges are tectonic in origin resulting from horizontal compressive stresses.

The largest known occurrence of wrinkle ridges on the terrestrial planets, observed within a distinct physiographic province, is on the Tharsis Plateau of Mars (6). The average spacing, evaluated in six provinces of the Tharsis ridge system, is 30 km (2,934 measurements), equal to the average spacing of the crosscutting wrinkle ridges of Hesperia Planum (7). There have been a number of buckling models proposed to explain the periodic nature of the wrinkle ridges (8,9,10,11,12) and some recent debate as to whether the lithosphere is involved in the deformation (thick-skinned) or not (thin-skinned). One reason for considering models that do not require wrinkle ridges be rooted in the lithosphere is the unlikelihood that stresses penetrating both the crust and lithosphere were involved in the deformation of ridged plains units well distant from Tharsis, particularly the many relatively small, isolated areas of ridged plains material that occupy topographic lows within intercrater plains.

In the models evaluated in this study, it is assumed that the ridged plains material behaves as both a single member and a multilayer with frictionless contacts, resting on a mechanically weak megaregolith substrate of finite thickness that has buckled at a critical wavelength of folding. The basement does not directly participate in the deformation that results in the ridges, thus no assumption of whole or partial lithosphere deformation is necessary to explain the periodic spacing. Free slip between layers is assumed based on the possible existence of mechanically weak interbeds in the ridged plains sequence separating groups of flows. Interbeds separating groups or units of flows are not uncommon within mare basalts on the Moon or in terrestrial continental flood basalt sequences (13,14,15) and may contribute to the localization of buckling (16). The rheologic behavior of the ridged plains and megaregolith are approximated by a linear elastic and linear viscous material. The models are examined for a range in: 1) the strength contrast between the ridged plains material and the underlying megaregolith of 100, 1,000 and 5,000; 2) thickness of the ridged plains material of 250 to 3,500 m; 3) thickness of the megaregolith of 1,000 to 5,000 m; and 4) number of layers (n) of 1 to 12. For the elastic case, wavelengths consistent with many of the observed spacings are obtained at critical stresses below the yield-strength of a basalt-like material for $n > 5$. For $n = 8$, wavelengths range from 27 to 42 km for thicknesses of the ridged plains material ranging from 1,900 to 3,500 m over a range in thickness of the substrate of 1,000 to 5,000 m and ratio in Young's modulus of 1,000 to 5,000. The cases of $n = 1$ (i.e., a single member) through 5 do not yield admissible wavelengths. At the upper limit of the model parameters, the average thickness of the ridged plains necessary to account

for the minimum average spacing of the ridges (20 km) is roughly 1,700 m. If the ridge spacing is the result of elastic buckling, the relatively high contrast in Young's modulus required ($\geq$ 1,000) is only possible if there were high pore-fluid pressure within the megaregolith at the time of deformation that reduced the effect of the overburden.

Over the same range in values of the parameters, viscous buckling is much less restricted than the elastic case. The observed wavelengths can be accounted for over almost the entire range of viscosity contrast, ridged plains material thickness and substrate thickness for either a single layer or a multilayer. The minimum average spacing of the ridges can be explained with a single layer (n = 1) at the lower limit of the estimated thickness of the ridged plains material (250 m), at the upper limit of the substrate thickness and viscosity contrast. In addition, viscous buckling is viable if the megaregolith were dry, water-rich or ice-rich at the time of deformation.

References Cited:

(1) Greeley, R., E. Theilig, J.E. Guest, M.H. Carr, H. Masursky and J.A. Cutts, *JGR, 82,* 4039-4109, 1977. (2) Scott, D.H. and K.L. Tanaka, *USGS Map I-1802-A,* Denver, Colo., 1986. (3) Watters, T.R., *JGR, 93,* 10,236-10,254, 1988. (4) Plescia, J.B. and M.P. Golombek, *GSA Bull., 97,* 1289-1299, 1986. (5) Sharpton, V.L. and J.W. Head, *Proc. LPSC IX,* 307-317, 1987. (6) Watters, T.R. and T.A. Maxwell, *JGR, 91,* 8113-8125, 1986. (7) Watters T.R. and D.J. Chadwick, *LPI Tech. Rep. No. 89-06,* 68-70, 1989. (8) Saunders, R.S. and T.E. Gregory, *NASA Tech. Memo. TM82385,* 93-94, 1980. (9) Watters, T.R. and T.A. Maxwell, *LPSC XVI,* 897-898, 1985. (10) Watters, T.R., *Fourth International Conference on Mars,* 206-207, 1989. (11) Zuber, M.T. and L.L. Aist, *LPSC XX,* 1261-1262, 1989. (12) Zuber, M.T. and L.L. Aist, submitted to *JGR,* 1989. (13) Peeples, W.J., R.W. Sill, T.W. May, S.H. Ward, R.J. Phillips, R.L. Jordan, E.A. Abott, and T.J. Killpack, *JGR, 83,* 3459-3468, 1978. (14) Reidel, S.P., T.L. Tolan, P.R. Hooper, K.R. Fecht, M.H. Beeson, R.D. Bentley, and J.L. Anderson, *GSA Sp. Paper 239,* in press, 1989. (15) BVSP, 1286 pp., Pergamon Press, New York, 1981. (16) Watters, T.R., *GSA Sp. Paper 239,* in press, 1989.

DOMAINS OF REGIONAL PURE SHEAR ON THE TERRESTRIAL PLANETS.

Thomas R. Watters and Michael J. Tuttle, Center for Earth and Planetary Studies, National Air and Space Museum, Smithsonian Institution, Washington, D.C. 20560

Tectonic domains where major fold and thrust fault trends are transected by conjugate strike-slip faults have been documented within fold-thrust belts on the Earth (1,2). The geometric relationships between the structures is best explained by a pure shear mechanism because of the limited extent and lateral displacements of the strike-slip faults (see 2). Given a N-S directed compressive stress, the system of structures possible includes E-W trending first-order folds and first-order right-lateral and conjugate left-lateral strike-slip faults with an angle θ to the primary stress direction. The angle θ is constrained by the Coulomb-Navier criterion where θ is related to the coefficient of internal friction μ. For typical values of μ between 0.58 and 1.0, θ is in the range of 22.5°-30°.

Yakima Fold Belt, Columbia Plateau, Earth

The anticlinal ridges in the continental flood basalts of the Columbia Plateau (or Columbia Basin) are long, narrow, periodically spaced structures with broad relatively undeformed synclines. The anticlinal ridges are believed to be the result of initial buckling in response to a horizontal compressive load followed by dominantly reverse to thrust faulting (3). Numerous strike-slip faults have been mapped in the southern portion of the fold belt (4). The lateral displacement along the most extensive faults is typically small (< 1 km). The strike-slip faults can be classified as either tear faults, faults of limited extent or regional faults (5). As part of this study, over 80 lineaments have been mapped, 73 of which are located in the southern portion of the fold belt. Many of these correspond to previously mapped right-lateral strike-slip faults. The mean direction of the known and suspected strike-slip faults in the southern portion of the fold belt is N37°W. Taking the normal to the mean direction of the anticlines to be the approximate direction of the principal compressive stress, the mean direction of the known and suspected right-lateral strike-slip faults is within the range for θ. The anticlinal ridges of the Columbia Plateau are good analogs to first-order ridges in wrinkle ridge assemblages that occur in the ridged plains material on Mars (6).

Wrinkle Ridge Assemblages, Mars

Wrinkle ridges occur in smooth plains material that is inferred to be volcanic in origin. These ridges are also believed to form in response to horizontal compression with reverse or thrust faulting developed as a result of buckling (flexure-fracture) or buckling the result of reverse or thrust faulting (fracture-flexure) (6,7). If the ridged plains material has deformed in a similar style to the basalts of the Columbia Plateau, then strike-slip faults and their associated secondary structures may be common on Mars. Lineaments that transect wrinkle ridges have been found in medium and high resolution Viking Orbiter images. Some are comparable in scale to strike-slip faults associated with the anticlines on the Columbia Plateau. Lineaments of limited areal extent that sharply truncate both *en echelon* stepping and individual ridge segments are interpreted to be tear faults. Crosscutting lineaments of greater areal extent ($\leq$ 100 km) occur near or within the expected range for θ and are interpreted to be strike-slip

faults consistent with a domain of regional pure shear. Like their analogs on the Columbia Plateau, the strike-slip faults accommodate a portion of the relatively low bulk strain apparent in the ridged plains. Other evidence of strike-slip faulting on Mars has been recently reported by Forsythe and Zimbelman (8) and Schultz (9).

Ridge Belts, Venus

Parallel to subparallel ridges form the prominent ridge belts identified in Venera 15/16 images. Although the role of extension (10) and compression (11,12) in origin of the ridge belts is under debate, the similarity in morphology of the ridges to wrinkle ridges suggests that they are the result of horizontal compression. Frank and Head (11) describe some of the ridges as broad arches and compare them to arches associated with maria wrinkle ridges. Crosscutting lineaments are common in the ridge belts (11,12). These lineaments often occur in conjugate sets and evidence of strike-slip motion has been reported (11,12), however we observe little or no apparent displacement along the lineaments studied thus far. The areal extent, limited apparent displacement and the estimated values of θ determine for the lineaments are consistent with the development of strike-slip faults in a domain of regional pure shear. Based on the assumption that the morphology and fold geometry of the ridges is similar to that of wrinkle ridges, crude estimates of the bulk strain within the ridge belts in the Pandrosos and Ahsonnutli Dorsa regions are as high as 7% (see 6), as compared to a maximum of roughly 2% estimated bulk strain for ridged plains of Tharsis and 5% for the deformed basalts of the Columbia Plateau.

References Cited:

(1) Tirrul, R., I.R. Bell, R.J. Griffis and V.E. Camp, *GSA Bull., 94*, 134-150, 1983. (2) Sylvester, A.G., *GSA Bull., 100*, 1666-1703, 1988. (3) Watters, T.R., in *GSA Sp. Paper 239*, in press, 1989. (4) Anderson, J.L., Ph.D. dissertation, Univ. South. CA, 1987. (5) T.L. Tolan, J.L. Anderson and M.H. Beeson, this volume. (6) Watters, T.R., *JGR 93*, 10,236-10,254, 1988. (7) Plescia, J.B. and M.P. Golombek, *GSA Bull., 97*, 1289-1299, 1986. (8) Forsythe R.D. and J.R. Zimbelman, *Nature, 336*, 143-146, 1988. (9) Schultz, R.A., *Nature, 341*, 424-426, 1989. (10) Sukhanov, A.L. and Pronin, A.A., *Proc. LPSC XIX*, 335-348, 1989. (11) Frank, S.L. and J.W. Head, *Venus Geoscience Tutorial, LPI No. 708*, 13-14, 1989. (12) Kryuchkov, V.P., *LPSC XX*, 546-547, 1989.

ORIGIN OF CURVILINEAR GRABEN IN SOUTHWEST LUNAE PLANUM, MARS.

Thomas R. Watters and Michael J. Tuttle, Center for Earth and Planetary Studies, National Air and Space Museum, Smithsonian Institution, Washington, D.C. 20560

The southwest Lunae Planum region of the Tharsis Plateau is being mapped at the 1:500,000 scale as part of the Mars Geologic Mapping program. The western margin of the ridged plains and plateau plains units in this region is marked by a steep, 3 km high erosional scarp. The plateau units in this region are cut by sets of curvilinear graben that occur within a 150 km zone of the scarp. There are three sets of graben in the region, set A cuts Noachian cratered uplands, set B cuts Hesperian plateau material and set C cuts both Hesperian plateau and ridged plains material (see A, B and C, fig. 1). The graben in set A have a mean direction of N12°E and are partially covered by ridged plains material that embays the cratered uplands (fig. 1, see A). Graben set B cuts plains material that appears to be continuous with the ridged plains material but lacks wrinkle ridges (fig. 1, see B). The trend of many of these graben (mean direction N10°E) are parallel to those in the adjacent cratered uplands. This suggests that these graben are the result of reactivation of a preexisting extensional fabric.

The orientation of graben in set A and B is not consistent with any phase of Tharsis radial extension (1). Circumferential oriented extensional stresses are predicted in this region in isostatic adjustment models (2,3,4), however, the curvature of the graben suggests that they were part of a circular swarm with a radius of approximately 300 km. Circular graben swarms are not uncommon in the Tharsis region. The most likely origin of the extensional stresses is local uplift resulting from the emplacement of an intrusive body. If this is the case, the initial intrusion may have coincided with some of the earliest tectonic activity in the Tharsis region.

The third set of graben (C) cut ridges plains material forming non-orthogonal ridge-fault crosscutting angular relationships (fig. 1, see C). This clearly indicates that graben formation postdates the deformation that resulted in the wrinkle ridges (5). The orientation of the graben in set C (mean direction N49°E) is also not consistent with Tharsis radial extension. However, unlike the other graben sets, the C graben parallel the scarp (mean direction of scarp segments is N52°E). Although the graben in set C do not appear to be related to the other sets, the orientations of the graben in sets B and C become parallel where they cut the same unit (fig. 1, see arrow). This suggests that in this area, the graben in set C were influenced by the same preexisting extensional fabric. The parallel nature of the graben and scarp suggests that the two are related. Possible explanations are: 1) the graben influenced scarp retreat, or 2) graben formation was influenced by, or a result of, the scarp. Extensional stresses near the scarp will result from the release of confining pressure, however, the magnitude of the stress would be expected to decay rapidly with distance from the wall. Another possibility is that extensional stresses resulted from loss of support. If the ridged plains overlie a thick megaregolith that was exposed by erosion, material may have been removed by undercutting and/or sapping. A finite element analysis is planned to determine under what conditions, if any, graben could form at the observed distances from the scarp.

References Cited:
(1) Plescia, J.B. and R.S. Saunders, *JGR, 87,* 9775-9791, 1982. (2) Banerdt, W.B., R.J. Phillips, N.H. Sleep, and R.S. Saunders, *JGR, 87,* 9723-9733, 1982. (3) Banerdt, W.B., M.P. Golombek, and K.L. Tanaka, submitted to *Mars*, University of Arizona Press, Tucson, 1989. (4) Sleep, N.H. and R.J. Phillips, *JGR, 90,* 4469-4489, 1985. (5) Watters, T.R. and T.A. Maxwell, *Icarus, 56,* 278-298, 1983.

Fig. 1. Photomaps of southwest Lunae Planum. The three sets of graben in the region are marked A, B and C.

DISTRIBUTION OF STRAIN IN THE FLOOR OF THE OLYMPUS MONS CALDERA. Thomas R. Watters and D. John Chadwick, Center for Earth and Planetary Studies, National Air and Space Museum, Smithsonian Institution, Washington, D.C. 20560, and Michael C. Liu, Department of Astronomy, Cornell University, Ithaca, NY 14853

The Olympus Mons caldera is made up of six coalescing volcanic craters (fig. 1). Based on comparisons with terrestrial volcanoes, such as Mauna Loa, Hawaii (1, 2), the volcanic craters are interpreted to be the result of collapse of a solidified lava lake due to evacuation of the magma chamber during late-stage summit activity (3). The floors of several of the craters are characterized by a large number of deformational features in the form of graben and wrinkle ridges. The largest and oldest of the volcanic craters (crater 6, see 3), approximately 65 km in diameter, has a well developed circumferential graben system in the margins of the floor (fig. 1). Wrinkle ridges are present in the interior of the floor but have been sharply truncated by at least three successive collapse episodes.

The origin of the stresses that generated the observed structures is likely the result of subsidence of the central portion of crater floors (3). Using topography derived by Wu et al. (4), subsidence is evident across the floor of the large crater (fig. 2, 5X vertical exaggeration). The cause of the subsidence is presumed to be loss of support of the caldera floor by withdrawal of the underlying magma, probably the result of flank eruptions. In a finite element analysis, Zuber and Mouginis-Mark (5) have shown that compressive and extensional stresses compatible with the generalized location of the structures can be generated by subsidence. A detailed assessment of the location of the wrinkle ridges and graben relative to the topography is useful in refining such models.

The distribution of the circumferential graben on the floor of large crater is not uniform. Mouginis-Mark (3) notes that the widths of graben are greatest near the crater edge and narrow toward the center of the floor. The most extensive fracturing of the floor is on the southern edge, near the rim of the of crater 3 (fig. 1). The average slope of the floor in the area of these graben is roughly 4° (fig. 2), the largest slopes observed on the floor. On the northern edge, there are fewer graben and the average slope of the floor is less (roughly 3°). Thus, the areas of greatest slope and possibly greatest flexure of the floor correspond to areas with the greatest observed extension. This correlation supports the assumption that the structures are the result of downward displacement of the floor. As noted by Zuber and Mouginis-Mark (5), many of the wrinkle ridges occur in topographic lows. In contrast to the circumferential graben, the ridges are not strongly radially distributed, but are confined to a roughly E-W oriented trough (fig. 2). The most prominent wrinkle ridge on the crater floor is located close to the area of lowest elevation. The average slope of the floor in area of the ridges is $\leq 2°$. Preliminary estimates of the bulk horizontal shortening and extension in the crater floor, using average values of the shortening across the ridges (see 6) and the extension across the graben (see 7), are roughly compatible at 1.5-2.0 km. Based on the topography and the distribution of structures, the subsidence appears to have been asymmetric with greater downward displacement and deformation of the southern half of the floor.

References Cited:
(1) Carr, M.H., *JGR, 78,* 4049-4062,1973. (2) Greeley, R., *Geology, 1,* 175-180, 1973. (3) Mouginis-Mark, P.J., *Proc. LPSC XII*, 1981. (4) Wu, S.S.C., P.A. Garcia, R. Jordan, F.J. Schafer and B.A. Skiff, *Nature, 309,* 432-435, 1984. (5) Zuber, M.T. and P.J. Mouginis-Mark, *LPI Tech. Rep. No. 89-06,* 74-75, 1989. (6) Watters, T.R., *JGR, 93,* 10,236-10,254, 1988. (7) Golombek, M.P., *JGR, 84,* 4657-4666, 1979.

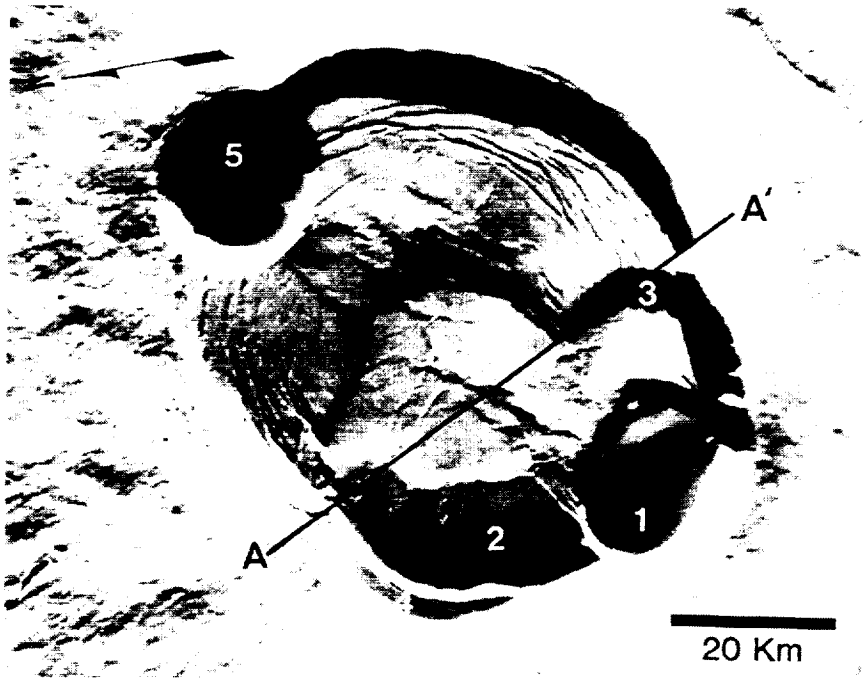

Fig. 1. Nested summit caldera of Olympus Mons.

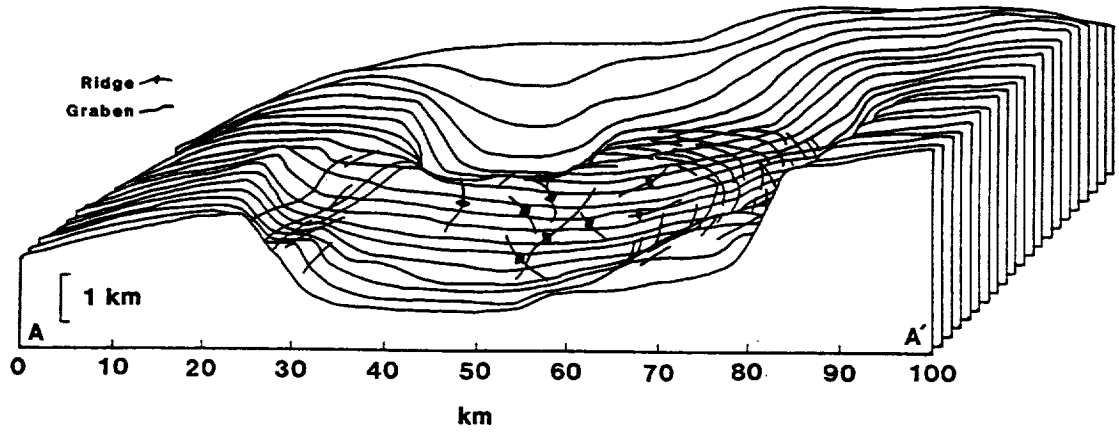

Fig. 2. Topographic profiles of a portion of the caldera with the location of prominent wrinkle ridges and graben.

SYMMETRY OF INFERRED STRESS FIELDS IN THE THARSIS REGION OF MARS. Thomas R. Watters and Michael J. Tuttle, Center for Earth and Planetary Studies, National Air and Space Museum, Smithsonian Institution, Washington, D.C. 20560, and Francis J. Kiger, Department of Geology and Astronomy, West Chester University, West Chester, Pennsylvania, 19383

Understanding the origin of the stresses that generated the radial fracture system and circumferential wrinkle ridge system on the Tharsis Plateau is key to unraveling the tectonic evolution of the region. Banerdt et al. (1,2) and Sleep and Phillips (3) have proposed models for the origin of the stresses and calculated stress trajectories that can be compared to the observed tectonic features. The stress fields predicted in these models are strongly radial to an area near Pavonis Mons. If these models are correct, the stress inferred from the structures should be strongly radial to this area.

The radial nature of the inferred stresses has been analyzed using a stereonet in a number of studies (4,5,6,7). In a recent study, Golombek (8), using graben data compiled by Plescia and Saunders (5) and ridge data subsampled into length-weighted vector means compiled by Watters and Maxwell (6), concluded that the graben and wrinkle ridges define a significantly radial system. With respect to the wrinkle ridges, this conclusion is in contrast to the findings of Watters and Maxwell (6) and is not the result of a net manipulation error as reported by Golombek (8). The method used by Golombek (8) involves fitting great circles with the correct angular relationship on the net to the vector normals. The resulting great circles are then geographically correct traces of the inferred principal stress on the surface. Watters and Maxwell (6) used the azimuth of the vector normals to fit the great circles. This method does not generate geographically correct traces of the inferred stresses, but can be used to test radial symmetry.

In an effort to address the question of the significance of the radial symmetry of the system of structures, a wrinkle ridge data set consisting of 1845 ridge segments and a graben data set consisting of 6841 fault segments is used in a beta analysis. Great circles that are geographically correct traces of the inferred principal stresses (8) are fit to each graben segment and the normals to each ridge segment. The 1.7 million intersections of the ridge data are distributed in a broad girdle with a maximum concentration of 5% per 1% area centered at approximately 5°S, 110°W (fig. 1). The 32 million intersections of the graben data are distributed in a symmetric pattern, elongated in a N-S direction with a maximum concentration of 12% per 1% area roughly centered at 3°S, 110°W (fig. 2).

The agreement between the locations of the maximum concentrations of intersections for the two systems of structures supports models where isostatic and flexural loading stresses result from the observed topography and gravity (1,2,3). However, in the isostatic case of Banerdt et al. (2), the predicted compressional stresses would result in a strongly radially symmetric ridge system (maximum concentration of 45% per 1% area located at roughly 5°N, 105°W). Even when the predicted stress trajectories are varied by as much as 10°, the maximum concentration does not approach 5%.

A possible explanation for the difference between the predicted stresses and those inferred from the observed structures is that some component of the total stress responsible for the wrinkle ridges is not accounted for in the models. Additional components of stress may have resulted from: 1) gravitationally induced down-surface slope stresses (9) generated when the

regional topographic slope was greater than at present, and 2) local and/or regional subsidence.

References Cited: (1) Banerdt, W.B., R.J. Phillips, N.H. Sleep, and R.S. Saunders, *JGR, 87,* 9723-9733, 1982. (2) Banerdt, W.B., M.P. Golombek, and K.L. Tanaka, submitted to *Mars,* University of Arizona Press, Tucson, 1989. (3) Sleep, N.H. and R.J. Phillips, *JGR, 90,* 4469-4489, 1985. (4) Wise, D.U., M.P. Golombek and G.E. McGill, *Icarus, 38,* 456-472, 1979. (5) Plescia, J.B. and R.S. Saunders, *JGR, 87,* 9775-9791, 1982. (6) Watters, T.R. and T.A. Maxwell, *JGR, 91,* 8113-8125, 1986. (7) Schultz R.A., *JGR, 90,* 1985. (8) Golombek, M.P., *LPSC XX,* 345-346, 1989. (9) Elliott, D., *JGR, 81,* 949-963, 1976.

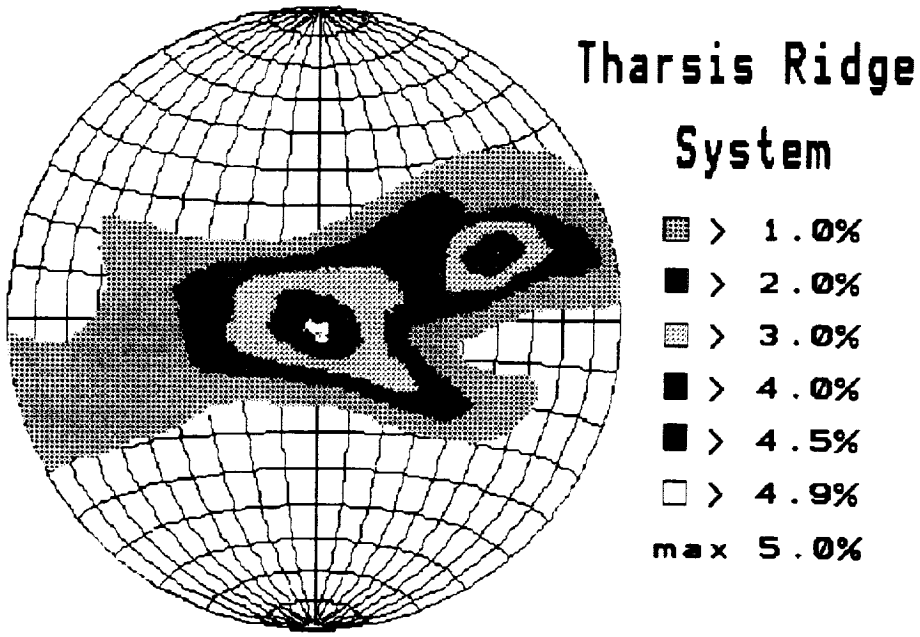

Fig. 1. Contours 1-2-3-4-4.5-4.9% per 1% area.

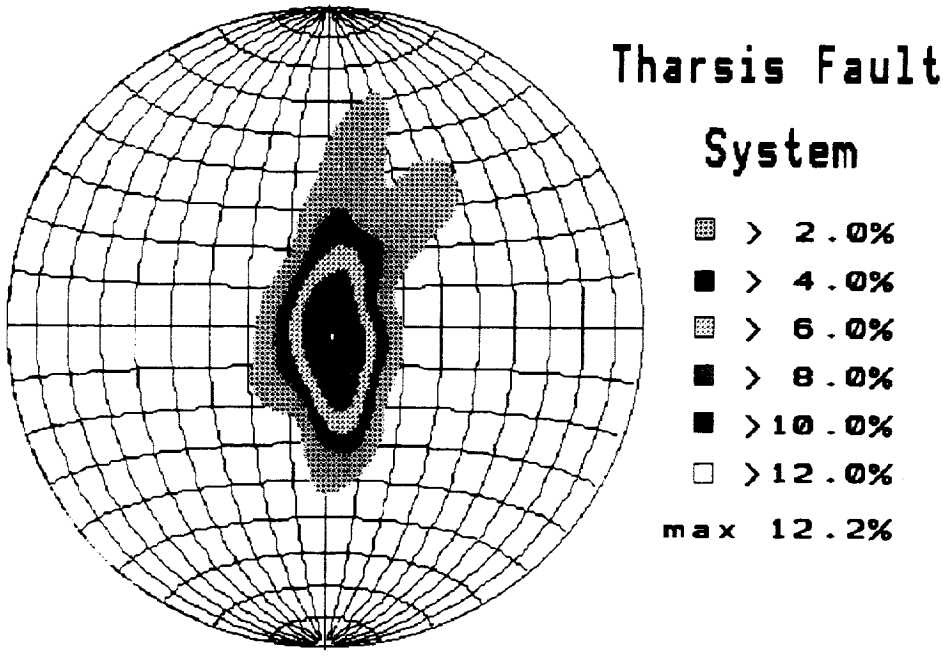

Fig. 2. Contours 2-4-6-8-10-12% per 1% area.

SIMULANTS FOR MARTIAN SURFACE MATERIALS; P. W. Weiblen, Space Science Center, U. of Minnesota, Minneapolis, MN 55455

Spectral-remote sensing observations and direct chemical and physical property measurements by the Viking Landers place constraints on the mineralogical and textural characteristics of the surface materials on Mars (1). Based on these data a number of terrestrial analogs for the fine dust components have been suggested, in particular, highly oxidized smectite clays with admixtures of iron oxyhydroxides and various sulfate minerals (2). Unfortunately, the available data on Martian materials is not sufficiently definitive to provide unambiguous guides to good choices for useful simulants which are already needed in the precursor research for future missions to Mars (Glaser, pers. comm., 1989).

Burns (3) noted that the chemistry and infrared spectra of hydrated, oxidized, iron-rich oikocrysts of olivine in Keweenawan (1.1 billion year old) olivine gabbros from the Midcontinent Rift (4) compare favorably with the Viking Lander and remote sensing data on Martian surface materials. The hydrated and oxidized iron-rich material has been referred to as "hisingerite" in the literature (5). It will be noted that compared to the Viking Lander data, the analyses of "hisingerite" are lower in alumina and lime. Addition of plagioclase would compensate for this difference. It is suggested that aeolian winnowing of hydrated and oxidized weathering products of basalt might produce such a mixture. It is interesting to note that in thin section the "hisingerite" is a bright red material. Analyses are in progress to characterize this material which appears to consist of a variety of ferric iron-rich clays associated with biotite, chlorite, and serpentine.

A simulant should be from a well-defined geologic site that is accessible and from which documented samples can be obtained. The occurrence of altered Keweenawan basalt on the North Shore of Lake Superior meets these criteria (4) and the necessary detailed characterization of collected material is now in progress to provide investigators with at least one possible simulant for Martian surface materials.

References: 1) Banin, A. (1988), LPI Technical Rpt. 88-07, 35,36. 2) Banin, A (1989) LPI Technical Rpt. 89-01, 15,17. 3) Burns, R.G. (1986) Nature, v. 320, #6, 55,56. 4) Weiblen, P.W., Saini-Eidukat, B., Miller, J.D. (1989) AGU Field Trip Guidebook T-345, 28th. Intl. Geol. Cong., pp. 43. 5) Whelan, J.A. & Goldich, S.S. (1961) Am. Min., v.46, 1412,1423.